Evaluation of Load Analysis Methods for NASA's GIII Adaptive Compliant Trailing Edge Project

Josue Cruz[1] and Eric J. Miller[2]

NASA Neil A. Armstrong Flight Research Center, Edwards, CA, 93523

The Air Force Research Laboratory (AFRL), NASA Armstrong Flight Research Center (AFRC), and FlexSys Inc. (Ann Arbor, Michigan) have collaborated to flight test the Adaptive Compliant Trailing Edge (ACTE) flaps. These flaps were installed on a Gulfstream Aerospace Corporation (GAC) GIII aircraft and tested at AFRC at various deflection angles over a range of flight conditions. External aerodynamic and inertial load analyses were conducted with the intention to ensure that the change in wing loads due to the deployed ACTE flap did not overload the existing baseline GIII wing box structure. The objective of this paper was to substantiate the analysis tools used for predicting wing loads at AFRC. Computational fluid dynamics (CFD) models and distributed mass inertial models were developed for predicting the loads on the wing. The analysis tools included TRANAIR (full potential) and CMARC (panel) models. Aerodynamic pressure data from the analysis codes were validated against static pressure port data collected in-flight. Combined results from the CFD predictions and the inertial load analysis were used to predict the normal force, bending moment, and torque loads on the wing. Wing loads obtained from calibrated strain gages installed on the wing were used for substantiation of the load prediction tools. The load predictions exhibited good agreement compared to the flight load results obtained from calibrated strain gage measurements.

Nomenclature

ACTE	=	adaptive compliant trailing edge
AFRC	=	Armstrong Flight Research Center
AFRL	=	Air Force Research Laboratory
B_W	=	wing aerodynamic bending moment, in-lbs.
BL	=	buttline
B_α	=	wing slope bending moment per degree angle of attack
b_W	=	wing span
C_B	=	wing aerodynamic bending moment coefficient, $\frac{B_W}{qS_Wb_W/2}$
C_{B_α}	=	wing aerodynamic bending moment coefficient, per degree angle of attack
C_L	=	lift coefficient
C_N	=	wing aerodynamic normal force coefficient, $\frac{N_W}{qS_W}$
C_{N_α}	=	wing aerodynamic normal force coefficient, per degree angle of attack
C_P	=	pressure coefficient
C_T	=	wing aerodynamic torque coefficient, $\frac{T_W}{qS_Wc_W}$
C_{T_α}	=	wing aerodynamic torque coefficient, per degree angle of attack
c_W	=	wing chord
CFD	=	computational fluid dynamics
CG	=	center of gravity
ERA	=	Environmentally Responsible Aviation
FLL	=	Flight Loads Lab

---

[1]Aerospace Engineer, NASA Armstrong, P.O. Box 273/Mail Stop 48202A Edwards, CA 93523, AIAA nonmember.
[2]Aerospace Engineer, NASA Armstrong, P.O. Box 273/Mail Stop 48202A Edwards, CA 93523, AIAA member.

GAC	=	Gulfstream Aerospace Corporation / Grumman Aerospace Corporation
IB TS	=	inboard transition surface
N_W	=	wing aerodynamic normal force, lb.
N_Z	=	aircraft normal acceleration, g
N_α	=	wing slope normal force per degree angle of attack
NASA	=	National Aeronautics and Space Administration
OB TS	=	outboard transition surface
psf	=	pounds per square foot
q	=	free stream dynamic pressure, lbs. /ft^2
RBS	=	rear beam station
S_W	=	wing surface area
SCRAT	=	SubsoniC Research Aircraft Testbed
T_W	=	wing aerodynamic torque, in-lbs.
TRL	=	technology readiness level
T_α	=	wing slope torque per degree angle of attack

I. Introduction

THE Adaptive Compliant Trailing Edge (ACTE) experimental flight research project was a joint effort between National Aeronautics and Space Administration (NASA), the U.S. Air Force Research Laboratory (AFRL), and FlexSys Inc. (Ann Arbor, Michigan) to flight-test the ACTE experiment. The objective of the project was to demonstrate a seamless adaptive compliant structural control surface in flight.[1] Wind-tunnel testing and small scale flight-tests of the compliant technology were conducted as an initial phase, but a full-scale compliant structure required flight-testing to provide data to show the technology could be transitioned to commercial industry.[2]

NASA Armstrong Flight Research Center (AFRC) has procured, modified, and instrumented a Gulfstream Aerospace Corporation, Georgia (GAC) GIII aircraft to increase the Technology Readiness Level (TRL) of promising new flight technologies. This aircraft is named the SubsoniC Research Aircraft Testbed (SCRAT)[3] (Fig. 1). The ACTE flap control surfaces were fabricated and installed to replace both existing Fowler flaps on the SCRAT. The ACTE flaps were tested at predetermined, fixed deflection angles for each flight, and remained fixed in that position for the duration of the flight. The flaps were flight-tested at deflection ranges of -2° and +30° (+ signifies down flap deflections). Predicted loads for this paper were completed at four ACTE flap settings (0°, 5°, 15°, and 30°).

The goal for the ACTE test program was to demonstrate the ACTE flaps in-flight at the greatest combination of Mach and dynamic pressure that was structurally allowable. This provided the need for external loads analysis in order to demonstrate the required margins of safety for the wing box structure. Table 1 shows ACTE flap operations limits.

Table 1. ACTE flap operational and design speeds limits.

ACTE flap position	Airspeed operational limit	Design airspeeds (+15 knot gust)
degrees	knots	knots
2	340	355
5	300	315
15	250	265
30	170	185

II. Aircraft Structural Composition

A. Baseline Wing Composition

The GIII is a 19-passenger business jet, with a max takeoff gross weight of 69,700 lb. The wing of the GIII was a design improvement that extended the GII leading edge 3 ft to the semi span, thus providing greater fuel capacity. The GIII has a swept wing with a wingspan of 77 ft 10 in. The origin of the swept wing reference frame is located on the wing root at 40-percent chord. The wing area is 934.6 sq ft and has an aspect ratio of 6. The wing has a three spar structure front spar, secondary front spar and rear spar, with an attached leading edge at the secondary front spar

(Fig. 2). The trailing edge is fitted with a single piece Fowler flap, flight and ground spoilers, and ailerons (Fig. 3). The flight and ground spoilers were removed for the ACTE flight testing to accommodate the ACTE modification.

B. ACTE Flap Composition

The ACTE structure is composed of four primary components. Figure 4 shows the four ACTE components. The main flap spans 168 in and is the main lifting surface. The inboard transition surface (IB TS) and outboard transition surface (OB TS) each span 24 in and blend the main flap structure into the inboard and outboard wing structure. Closeout panels were added around the ACTE boundary to create the seamless structure.

III.   Instrumentation

A. Static Pressure Ports

The GIII wing was instrumented with a total of 141 surface pressure ports, 47 ports on each buttline (BL) ~136 in, ~201 in, and ~269 in. Seven pressure ports were drilled in the wing leading edge at each buttline. Forty pressure ports on each buttline were integrated to vinyl tubing adhered to the top and bottom surfaces of the wing.[3] The three spanwise runs are located within the main flap surface area. A photo of the vinyl tubing location can be seen on Fig. 5.

B. Wing Strain Gages

Load calibrated strain gages were installed on the left wing for measuring normal force, bending moment, and torque loads. The load calibration methodology utilized on the GIII wings replicates the techniques used on past load calibration projects.[4,5] The wing box structure was instrumented at two wing span stations located at Rear Beam Station (RBS) 152 and RBS 343. The measurement axes for bending moment and torque loads are oriented along and perpendicular to the 40-percent wing chord, as shown in Fig. 6. The strain gages were installed at RBS 152 and RBS 343 for ease of alignment of the gage orientations. The data presented in this report are only for RBS 152.

Each measurement station was instrumented with 16 metallic foil strain gages. The top left schematic in Fig. 6 shows 14 metallic foil strain gages. Two additional spare shear gages were added to the forward and rear spars of the wing. Load equations were derived using linear regression methods by correlating applied known loads to the wing with the output of the strain gage sensors during load application. Figure 7 shows the aircraft supported by airbags for the strain gage loads calibration testing to minimize the influence of the main gear reaction loads into the derivation of the load equations.[6] The wing interface ACTE fittings were also calibrated for monitoring loads into the wing, and Ref. 7 provides information about the calibration.

The derived load equations were set equal to the weight of the wing outboard of the measurement station for the ground rest state with no fuel in the wings. Without this initial zero point, the flight data would have an offset error. The derived load equations represent a net flight load which includes aerodynamic pressure loads and inertial loads. The inertial loads include wing structural weight and fuel weight outboard of the measurement station.

C. SCRAT Instrumentation System

Normal force, bending moment, and torque loads were monitored during the ACTE flight-test. The SCRAT aircraft instrumentation system collected data from sensors positioned throughout the aircraft. The data were recorded onboard and transmitted to the ground for real-time monitoring in the control room. The aircraft instrumentation system has 16-bit resolution, allowing adequate range and resolution in the measurements. The instrumentation system is configured for monitoring approximately 6000 parameters at a range of 1 to 20,000 samples per s. The wing loads were monitored at 100 samples per s.

IV.   Flight-Test Envelope

The ACTE flaps were flight-tested to a max airspeed of 340 KCAS and Mach 0.75. The altitude was limited to 40,000 ft to minimize testing requirements (Fig. 8). The stall limit with the ACTE flaps installed was based on each static flap setting and aircraft gross weight. A range of maneuvers were flown at each test point which included steady state trim points, doublets and raps in all three axes, pushover-pullups, and wind-up turns. The aircraft was limited to a normal acceleration of 0 g to 2.0 g for all test conditions. This paper presents data for steady-state maneuvers at 1.0 g, and 0.0 to 2.0 g pushover-pullup data.

V.   Modeling and Simulation Procedure

The purpose of the CFD study was to validate the TRANAIR[8] and CMARC[9] analysis tools for predicting in-flight loads. The objective was to ensure that the change in wing loading due to the addition of the ACTE flap would not

exceed the existing GIII wing structure capability. The results in this paper will show analysis comparisons of dynamic pressures from 92 to 255 pounds per square foot (psf) in TRANAIR and CMARC. The CFD-based simulations were compared to flight data results from ACTE flights. A flow chart of this process is presented in Fig. 9.

A. Computational Fluid Dynamics Models

Pressure load models were generated in the two computational codes mentioned above. A panel code called CMARC (Fig. 10) was used. This code is ideal for quick and accurate analysis of pre-stall, low subsonic flow. The aircraft grid was modeled as a half configuration with a symmetry plane. The grid consisted of a total of 2463 surface panels, from which 1174 surface panels corresponded to the wing and winglet. Each CFD CMARC coarse structured grid was generated by LOFTSMAN and is composed of the fuselage, wing, and vertical and horizontal tails. A separate grid is created for each ACTE flap deflection, for a total of six different grids. The elevator control surface is modeled through the rotation of the panel normal up to about 15 deg, and does not require re-gridding.[9]

A higher fidelity analysis approach using TRANAIR (Fig. 10) was analyzed for each case. TRANAIR is a non-linear full potential solver directly coupled with an integral boundary layer solver. Aerodynamic Grid and Paneling System (AGPS) was used to generate the surface grid representation of the GIII aircraft with the ACTE model. Similar to CMARC, the TRANAIR aircraft grid was modeled as a half configuration with a symmetry plane. The final grid for TRANAIR was approximately 0.9 million cells in the entire domain. There were approximately 72,500 surface panels, from which 32,000 surface panels corresponded to the wing and winglet. The TRANAIR structured surface grid is more detailed than the CMARC grid; it models the fuselage, wing, vertical and horizontal tails, engine, and engine pylon. A separate grid was created for each ACTE flap deflection, for a total of six different grids. The elevator control surface is modeled through the use of the transpiration method in TRANAIR.

B. Inertia Loads Models

In addition to the computational models used to generate the pressure loads on the wing, an inertial load model was needed for the net loads analysis. The mass properties of the ACTE flap and the wing were obtained from two separate sources. The ACTE flap mass distribution is from NASA's analysis. The wing mass distribution modeling was completed from information outlined in the GAC loads report. The wing and winglet were discretized into multiple panels and assigned a weight to each panel for multiple fuel configurations. Figure 11 shows an example of the wing grid, where dark circles represent the edge points of the panels, and the empty circles represent centroid locations.

C. Analysis Conditions

From the flight data collected, the CFD lift coefficient (C_L) and trimmed conditions were identified based on the weight of the aircraft, the dynamic pressure, normal acceleration (N_Z), and altitude at steady state conditions. The center of gravity (CG) was also calculated from these steady state maneuvers. A rigid-body approach was primarily used for the analysis which provides a conservative estimate of the aircraft loads. While incorporating elastic-body effects could result in more accurate load predictions, it was determined that the rigid-body analysis was sufficient to meet project requirements and the more conservative rigid-body load predictions would be sufficient in all the test cases. The steady state loads test points at 1.0 g limit were conducted at the following conditions, shown in Table 2.

Table 2. Steady state flight conditions.

	Mach	Altitude, ft	ACTE deflection, deg
1.	0.30	10,000	0
2.	0.40	10,000	0
3.	0.50	10,000	0
4.	0.30	10,000	5
5.	0.40	10,000	5
6.	0.50	10,000	5
7.	0.30	10,000	15
8.	0.40	10,000	15
9.	0.55	20,000	15
10.	0.30	10,000	30

D. Calculation of Wing Loads

The integrated loads consisting of the normal force, bending moment, and torque were obtained from a load distribution on the wing (aero and inertial). The aerodynamic loads distribution was calculated from predicted pressure distribution through analysis in both the CMARC and TRANAIR codes. Since the pressure distribution on the wing is obtained from CFD results, the pressure in effect was discretized into panels similar to the CFD discretization along the wing. Each panel had an associated pressure coefficient value (C_P), and X, Y, Z coordinates of the corner nodes. As stated in the Inertia Loads Models section above, the inertial load distribution was obtained from analysis of the mass properties of the wing. Similar to the pressure distribution, the mass properties of the wing were discretized into multiple panels.

The pressure and inertial loads were distributed across the span of the wing and segmented into three parts: wing normal force (N_W), bending moment (B_W), and torque (T_W).[10] The origin of the swept wing reference frame is located on the wing root at 40-percent chord. The Y-axis is rotated such that the axis runs parallel to the 40-percent wing chord line. This reference frame is used in the computation of the swept normal force, bending moment, and torque loads.

The normal force wing loading was applied as an integrated span load (aero and inertial) acting normal to the wing plane in the upward direction. The bending moment was calculated about a line perpendicular to the 40-percent chord swept axis load station, caused by the normal force outboard of that line. The torque loads were calculated about the 40-percent chord swept axis, caused by the normal force outboard of the swept axis. Positive loads are leading edge up.

VI. Results

A. Pressure Coefficient Results

CMARC and Viscous TRANAIR computations were analyzed at the flight conditions identified in Table 2. The C_P distributions were extracted from the CFD solutions at each of the three buttlines (~136 in, ~201 in, and ~269 in) and the corresponding C_P values were recorded at identical buttline locations for the flight-test data. Due to the large number of graphs, only the mid-BL ~201 data are presented in this paper. Buttline ~136 and ~269 displayed similar trends as BL ~201. The black full and empty circle symbols correspond to flight data (upper and lower pressures). The round dots correspond to CMARC CFD data, and the dashed lines correspond to TRANAIR CFD data.

Overall, the CFD pressures correlated well to the flight data for most cases. For the condition ACTE flap setting 0 deg at Mach 0.3, and Mach 0.4 (Figs. 12 and 13), the experimental results show that the estimated CFD pressures at the leading edge did not correspond very well at some of the points. One possible cause could be that the CFD is not exactly predicting the flight angle of attack. Another possibility is not enough pressure ports on the GIII wing leading edge to compare against CFD data. Figure 14, ACTE flap setting 0 deg at Mach 0.5, presented a better trend with flight data. In Fig. 15, ACTE flap setting 5 deg at Mach 0.3, the C_P did not match the leading edge as well. In Figs. 16 and 17, ACTE flap setting 5 degrees at Mach 0.4 and Mach 0.5, the CFD simulation correctly predicts the pressure peak at the leading edge. In Figs. 18 through 20, the same trend can be seen on the ACTE flap setting 15 deg, where simulation correctly predicts the leading edge pressure at x/c=0.0 for all flight conditions. Figure 18, the trailing edge for ACTE flap setting 15 deg at Mach 0.3, shows larger changes in pressure on both the upper and lower surfaces; this behavior is not captured well by the CFD simulations, and to a lesser extent, Mach 0.4 and Mach 0.5 (Figs. 19 and 20).

Figure 21 shows the results of the ACTE flap setting at 30 deg deflection. TRANAIR and CMARC both used inviscid solution. TRANAIR ACTE flap setting 30 deg viscous solution did not converge. Results show that the CFD profile did not match the trailing edge. There is flow separation from the flight data beyond x/c=0.90, which the CFD is not able to simulate. As a result, there is disagreement at the trailing edge. The leading edge also shows disagreement with the CFD, and this disagreement was expected due to the inviscid solutions. As previously stated, the CFD lift coefficient (C_L) and trimmed conditions were identified based on the weight of the aircraft, the dynamic pressure, normal acceleration (N_Z), and altitude at steady state conditions. In both codes, the inviscid solution achieved the C_L and trimmed conditions with a lower angle of attack. As a result, the angle of attack from the CFD was smaller in magnitude than the flight angle of attack. The analysis for the ACTE flap setting at 30 deg is a clear example of the limitations of these tools.

B. Wing Loads (Normal Force, Bending Moment, and Torque)

In Figs. 22 through 24, ACTE flap setting 0, 5, and 15 deg, the normal force coefficient results show good agreement at all conditions. For all ACTE flap settings, Mach 0.3 presented the lowest percentage error from 1.22 percent to 8.42 percent. As the Mach increases, the percentage error increases. The percentage error for Mach 0.4

was 6.84 percent to 12.36 percent, and for Mach 0.5 the percentage error was from 1.06 percent to 22.13 percent. ACTE flap setting 30 deg is not presented due to the limited flight test data and predicted data. In Figs. 25 through 27, the bending moment results show a higher percentage difference when compared to flight data. The lowest percentage error was at Mach 0.3 and ACTE flap setting to 0 deg, with 8.74-percent error, and the highest was at Mach 0.5 ACTE flap setting 15 deg, with 25.81-percent error. The same trend can be seen on the torque loads where simulation incorrectly underpredicts or overpredicts the values for the three ACTE flap settings (Figs. 28 through 30). The percentage error for torque loads was beyond 25 percent. The differences in bending moment and torque are possible due to elasticity effects that were not accounted for in this work. Further CFD analyses would be required to improve the correlation between CFD moments and flight data.

C. Wing Slopes and Loads Coefficients at Different ACTE Flap Settings

Figures 31 through 33 present the calculated wing slopes at Mach 0.3 taken from pushover-pullup maneuvers flown up to 2.0 g, including flight-test data which was not predicted in CFD. The load coefficients slopes were determined from the normal force, bending moment, and torque loads in units of load per degree angle of attack. As the figures show, the agreement between the flight data and predicted loads match well; however, differences can be seen where the CFD underpredicts or overpredicts some of the load slopes.

Figures 34 through 36 present Mach 0.3 coefficient data at different ACTE flap settings. The data show good correlation for the lower ACTE flap settings. As the flap deflection increases, the torque loads on the wing increase in the negative direction, as would be expected. At the higher ACTE flap settings the CFD data shows disagreement with the flight data. As stated earlier for ACTE flap setting at 30 deg, the solution for both tools, TRANAIR and CMARC, was inviscid. The inviscid solution shows larger changes in pressure on both the upper and lower surfaces (Fig. 21). As a result, the loads coefficients are larger than the flight data.

VII. Conclusions

The study utilized TRANAIR and CMARC. The CFD-based simulations were compared to flight data from a flight test conducted at NASA Armstrong for ACTE flap settings 0, 5, 15, and 30 deg. The purpose for this work was to substantiate NASA analysis processes for predicting normal force, bending moment, and torque loads on the GIII wing at RBS 152. The predicted wing loads were compared against calibrated strain gage wing load data located on the inboard measurement station of the GIII wing. Furthermore, CFD C_P values were validated using flight-test pressure data.

The CFD simulation matched the experimental C_P profile well and, as expected, this led to good agreement in the predicted normal force, except for ACTE flap setting 30 deg where the C_P did not match the flight data. The CFD-based analysis for ACTE flap setting 0, 5, and 15 deg, had good agreement with bending moment and torque, however, further analysis is necessary to have better results. The addition of aerolasticity effects could possibly reduce the dissimilarities in bending moment and torque results. The results of this study show that the CFD and inertia tools utilized for this analysis could be used for future studies of wing loads applications.

Acknowledgments

References

[1]Miller, E. J., Lokos, W. A., Cruz, J., Crampton, G., Stephens, C. A., Sridhar, K., Ervin, G., Flick, P. "Approach For Structurally Clearing An Adaptive Compliant Trailing Edge Flap For Flight," 46th SFTE International Symposium, Lancaster, California, September 2015.

[2] Sridhar, K., Osborn, R., Ervin, G., Flick, P., and Paul, D., "Mission Adaptive Compliant Wing – Design, Fabrication and Flight Test," *Symposium on Morphing Vehicles*, RTO-MP-AVT-168, Lisbon, Portugal, 2009.

[3]Baumann, E., Hernandez, J., and Ruhf, J., "An Overview of NASA's SubsoniC Research Aircraft Testbed (SCRAT)," AIAA-2013-5083, August 2013.

[4]Skopinski, T.H., Aiken, W.S. Jr., and Huston W.B., "Calibration of Strain-Gage Installations in Aircraft Structures for the Measurement of Flight Loads," NACA Report 1178, 1954.

[5]Jenkins, J.M., and DeAngelis, V.M., "A Summary of Numerous Strain-Gage Load Calibrations on Aircraft Wings and Tails in a Technological Format," NASA-TM-4804, 1997.

[6]Lokos, W.A, Miller, E.J., Hudson, L.D., Holguin, A.C., Neufeld, D.C., and Haraguchi, R., "Strain Gage Loads Calibration Testing With Air Bag Support for the Gulfstream III SCRAT Aircraft," AIAA-2015-2020, 2015.

[7]Miller, E.J., Holguin, A.C., Cruz, J., and Lokos, W.A., "Strain Gage Load Calibration of the Wing Interface Fittings for the Adaptive Compliant Trailing Edge Flap Flight Test," AIAA 2014-0277, January 2014.

[8]TRANAIR++, CALMAR Research Corporation, http://www.calmarresearch.com/NF/STG/Tranair/Tranair.htm, accessed August 3, 2015.

[9]CMARC, Personal Simulation Works, http://www.aerologic.com/, accessed October 14, 2015.

[10]Lomax, T.L., *Structural Loads Analysis for Commercial Transport Aircraft: Theory and Practice*, AIAA Education Series, AIAA, Reston, Virginia, 1996.

Figures

Figure 1. Modified Gulfstream III is the test bed aircraft used for ACTE flexible-flap research.
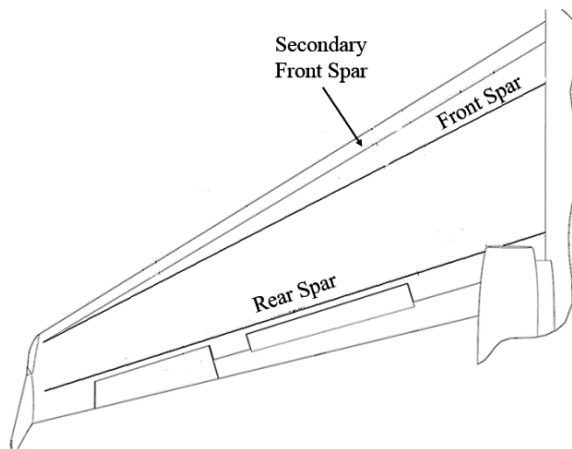
Figure 2. Left wing schematic with ACTE not installed.
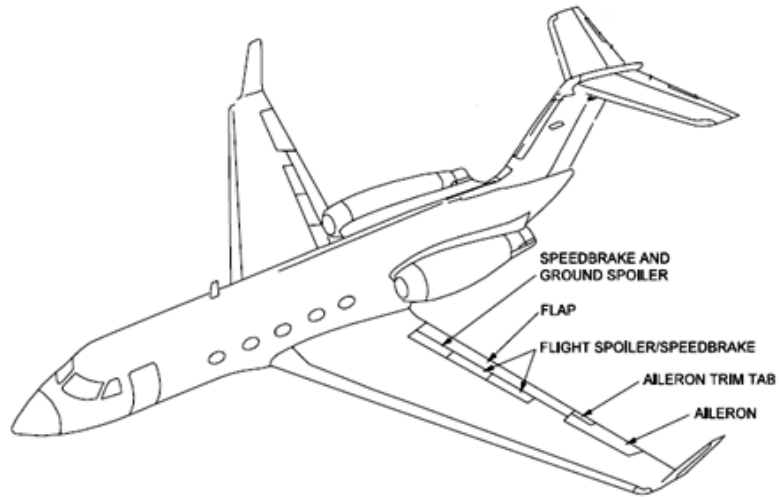
Figure 3. GIII wing control surfaces configuration without ACTE installed.
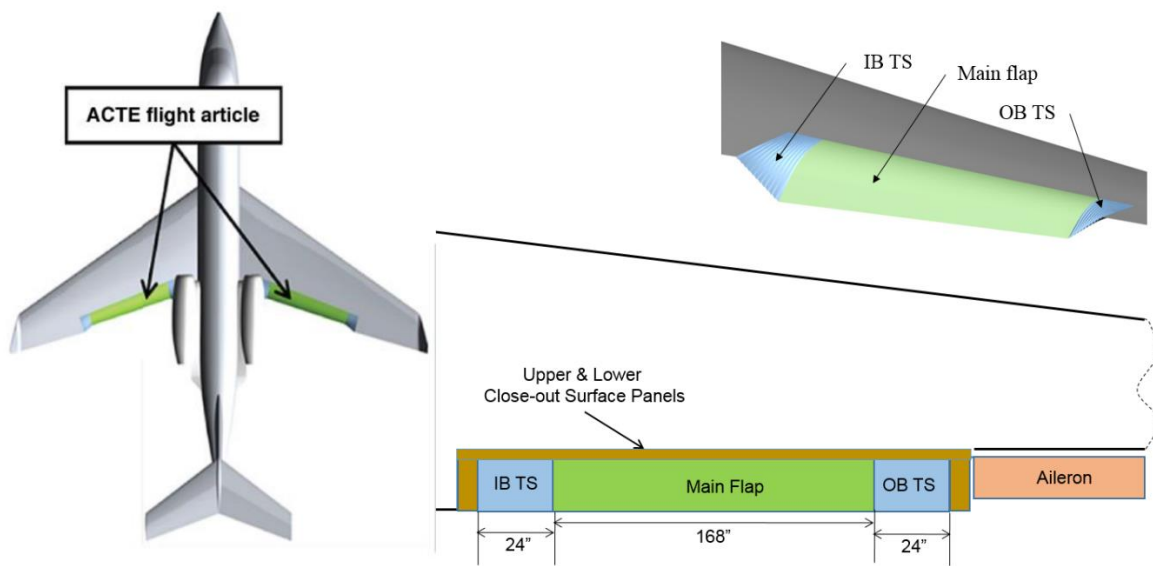
Figure 4. ACTE flap components as installed for flight-testing.

Figure 5. NASA's GIII inside the hangar.
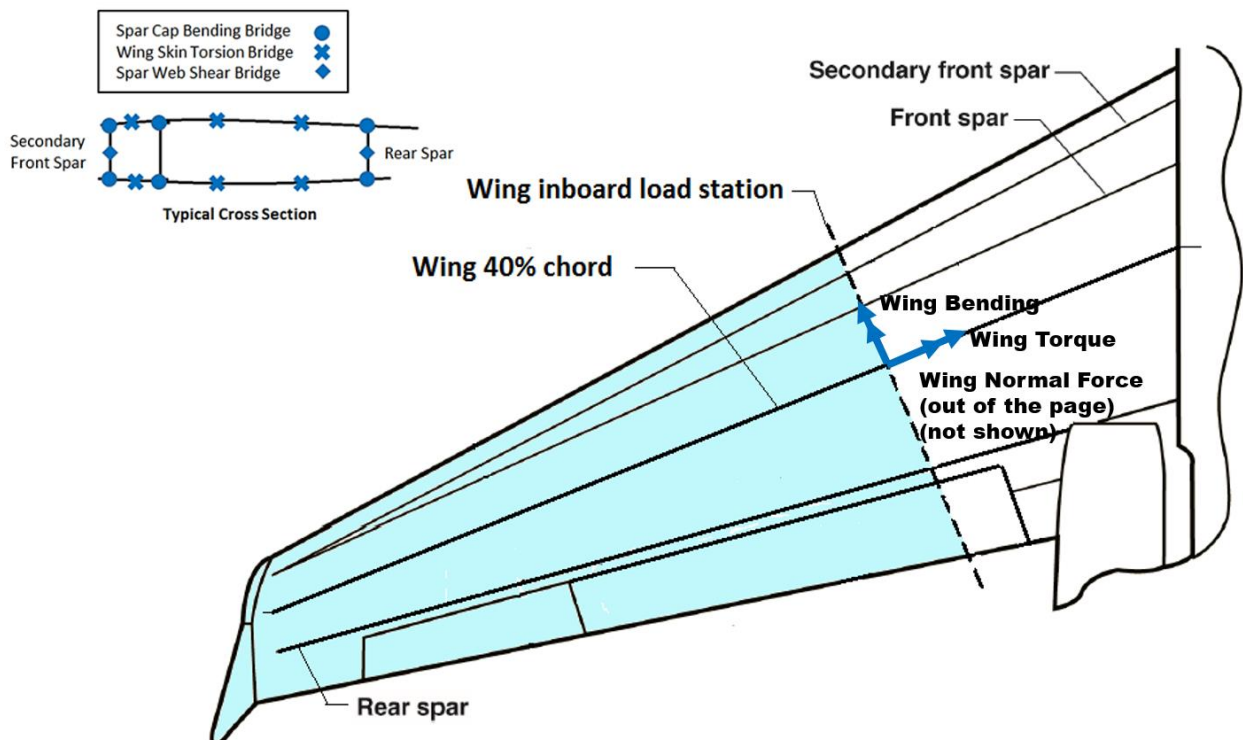
Figure 6. Loads definition on the ACTE wing.

Figure 7. Photograph of hydraulic up load case with aircraft supported on airbag.
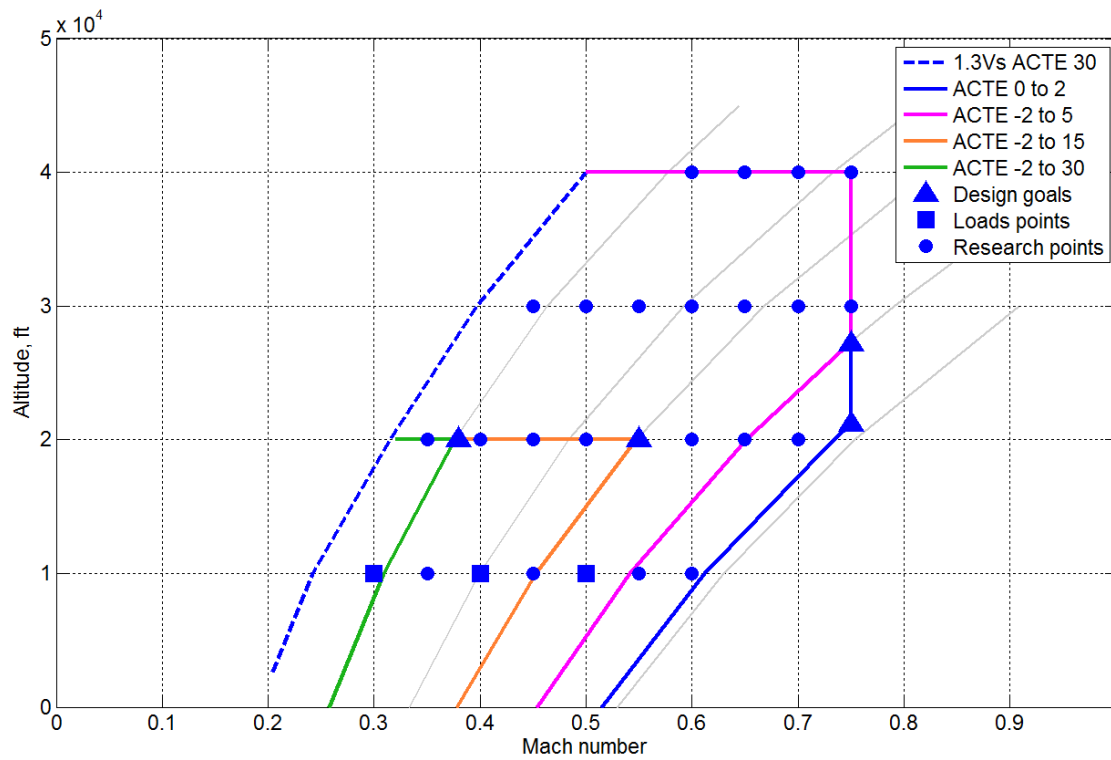
Figure 8. ACTE flight-test envelope.

American Institute of Aeronautics and Astronautics
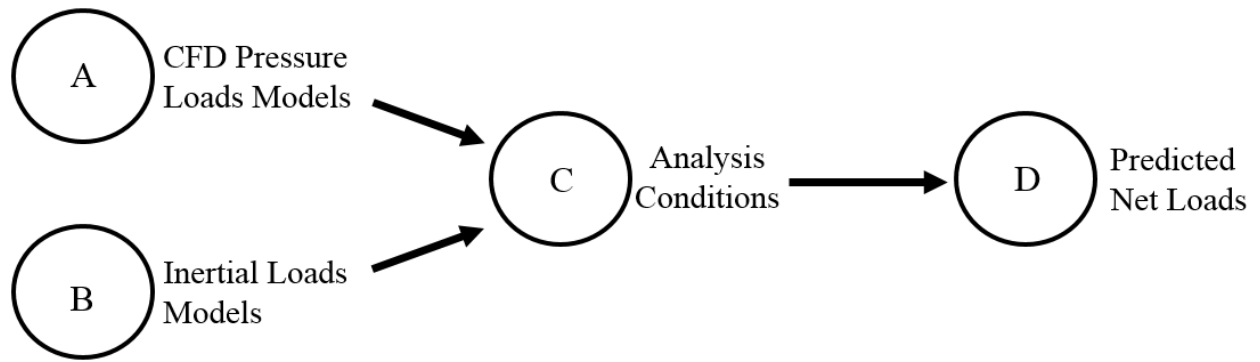
Figure 9. Loads prediction analysis flow chart.
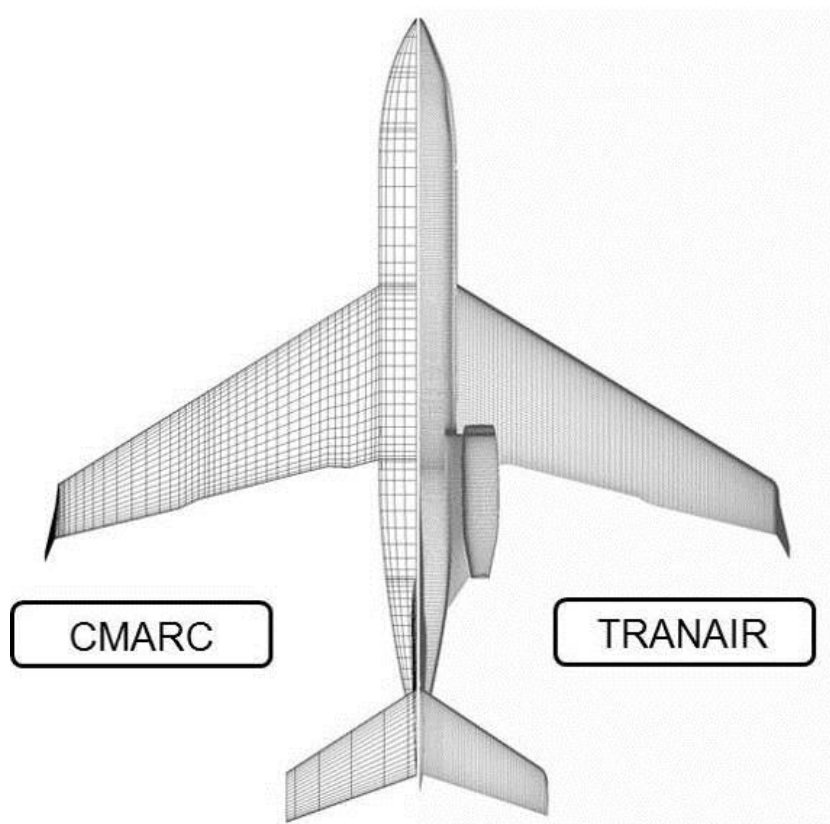
Figure 10. Computational grids for ACTE flap setting at 30°, CMARC (left) and TRANAIR (right).
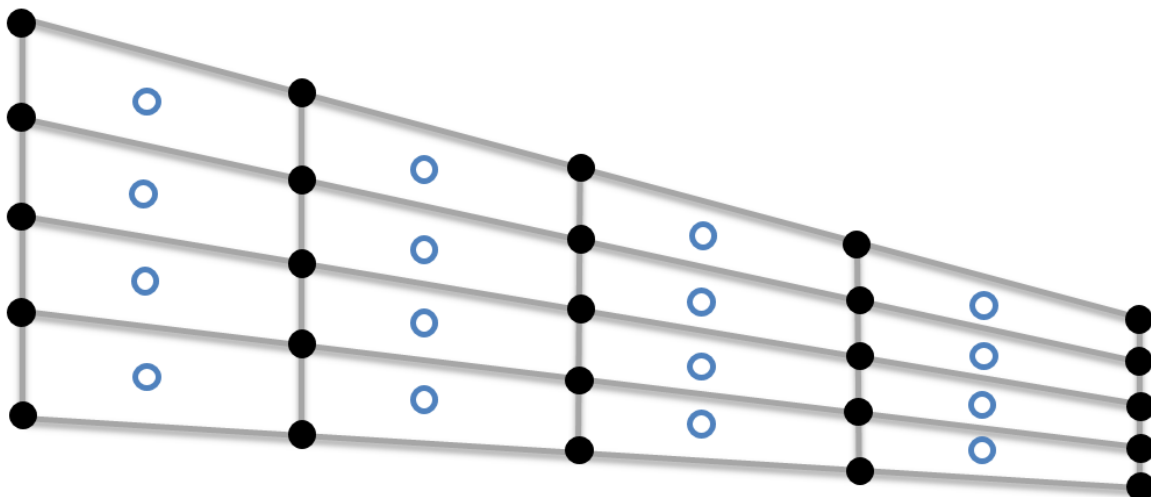
Figure 11. Example of wing grid with panel edges and centroid locations.
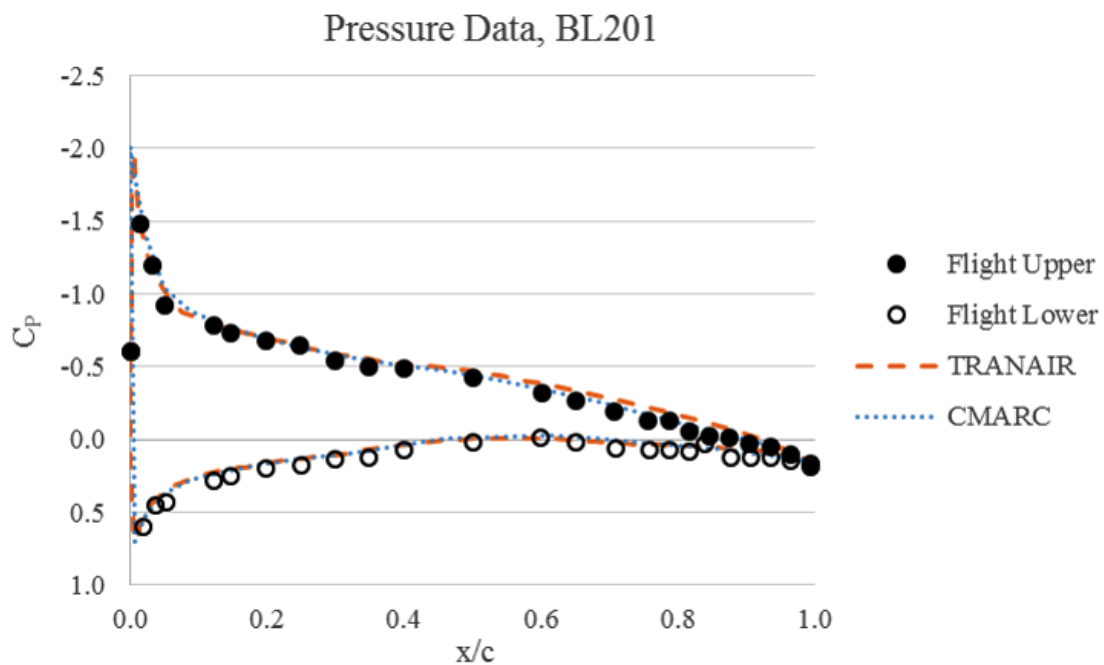
Figure 12. ACTE flap setting at 0 deg, Mach 0.3 at 10,000 ft.

American Institute of Aeronautics and Astronautics

Pressure Data, BL201
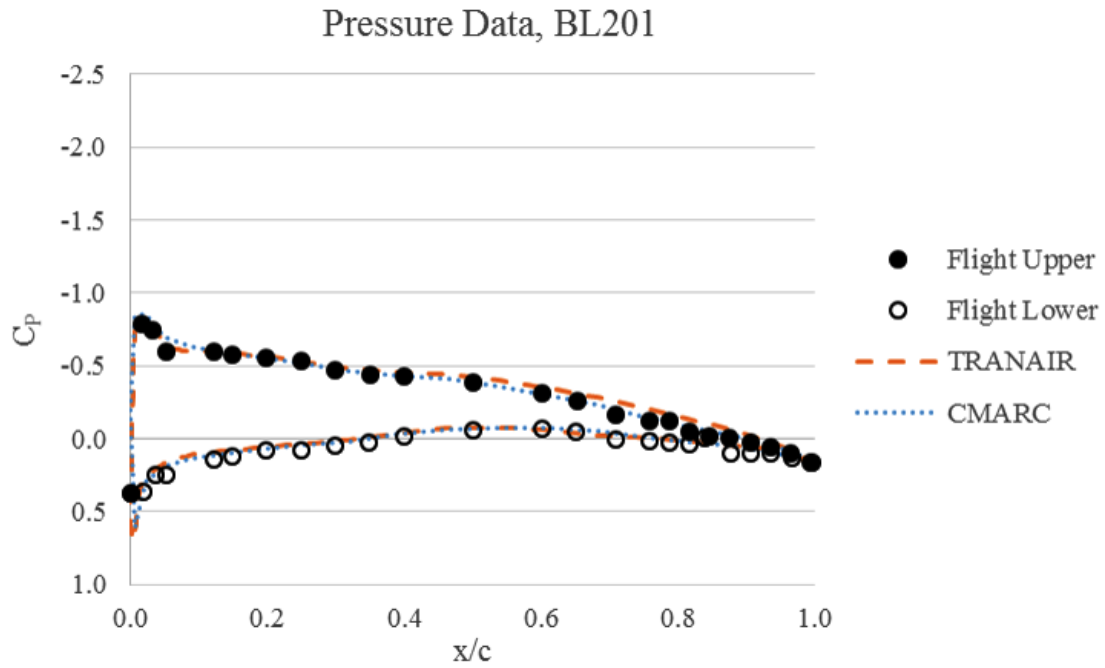
Figure 13. ACTE flap setting at 0 deg, Mach 0.4 at 10,000 ft.

Pressure Data, BL201
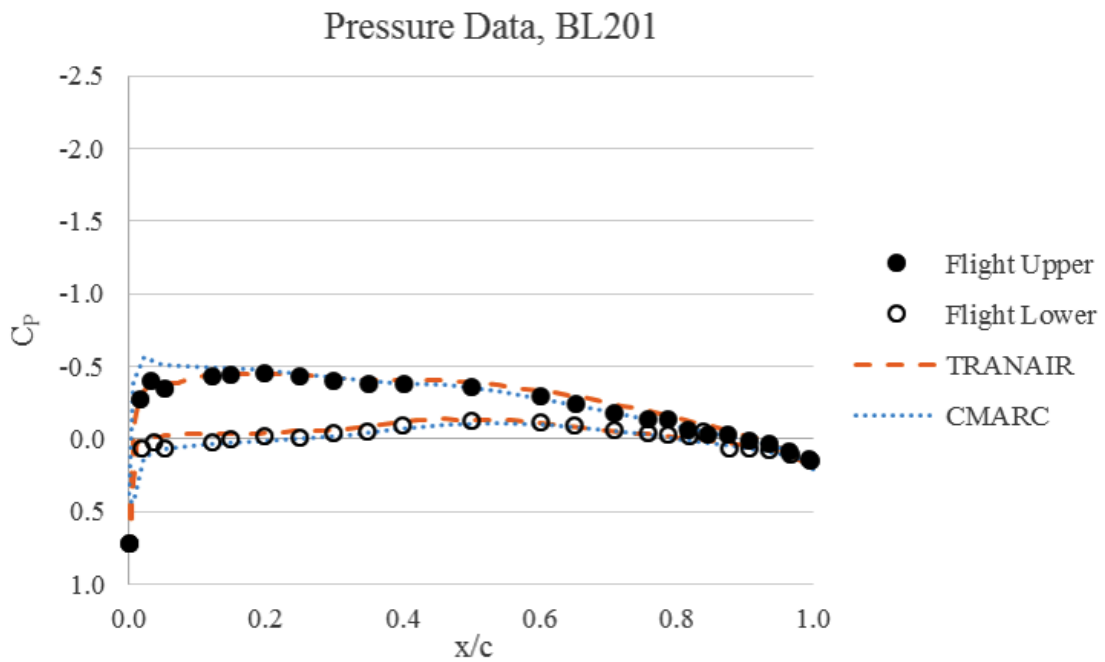
Figure 14. ACTE flap setting at 0 deg, Mach 0.5 at 10,000 ft.

American Institute of Aeronautics and Astronautics

Pressure Data, BL201
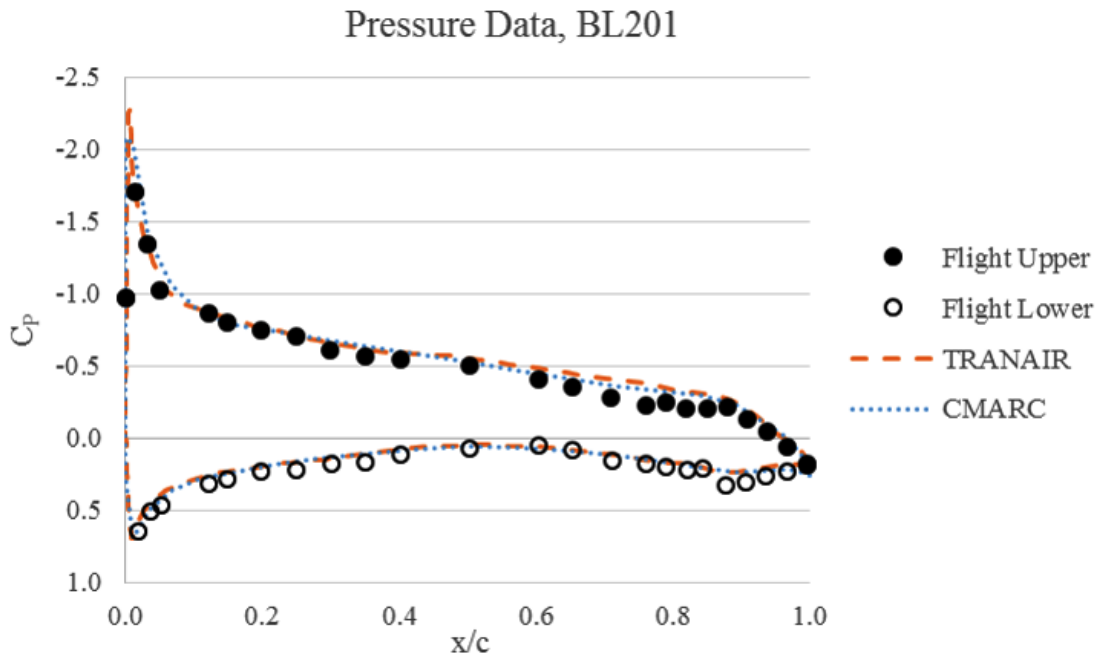
Figure 15. ACTE flap setting at 5 deg, Mach 0.3 at 10,000 ft.

Pressure Data, BL201
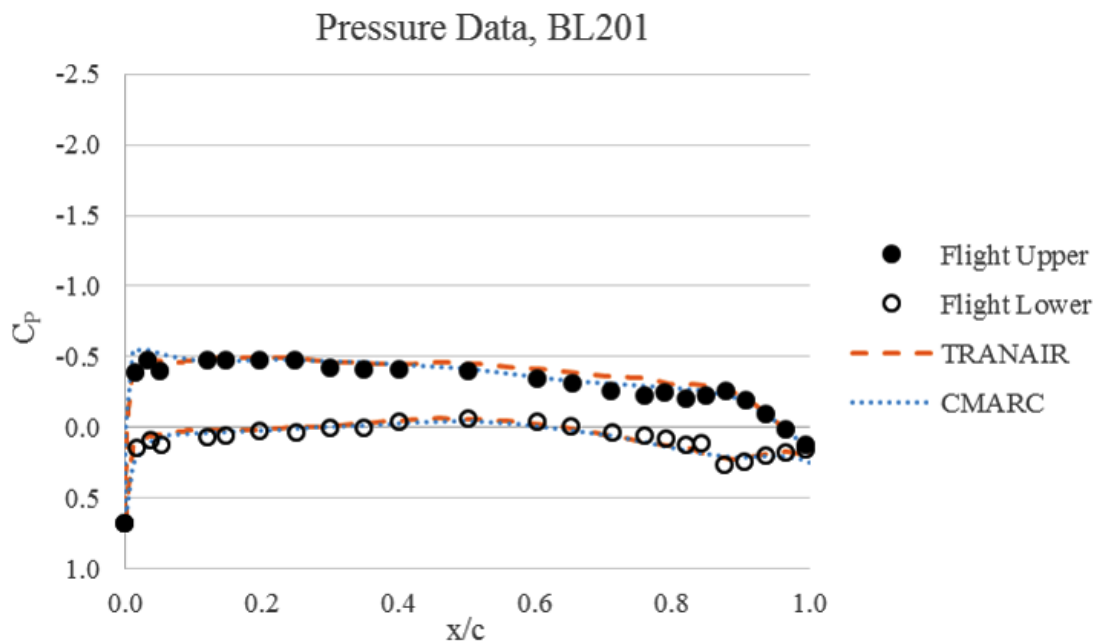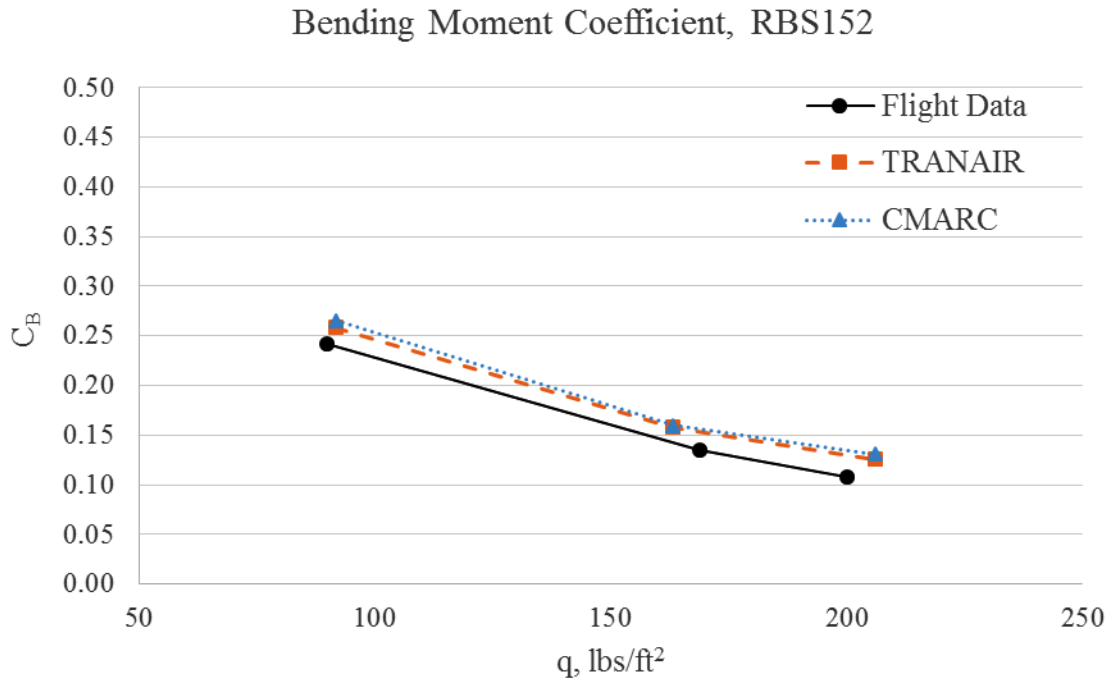
Figure 16. ACTE flap setting at 5 deg, Mach 0.4 at 10,000 ft.

Pressure Data, BL201
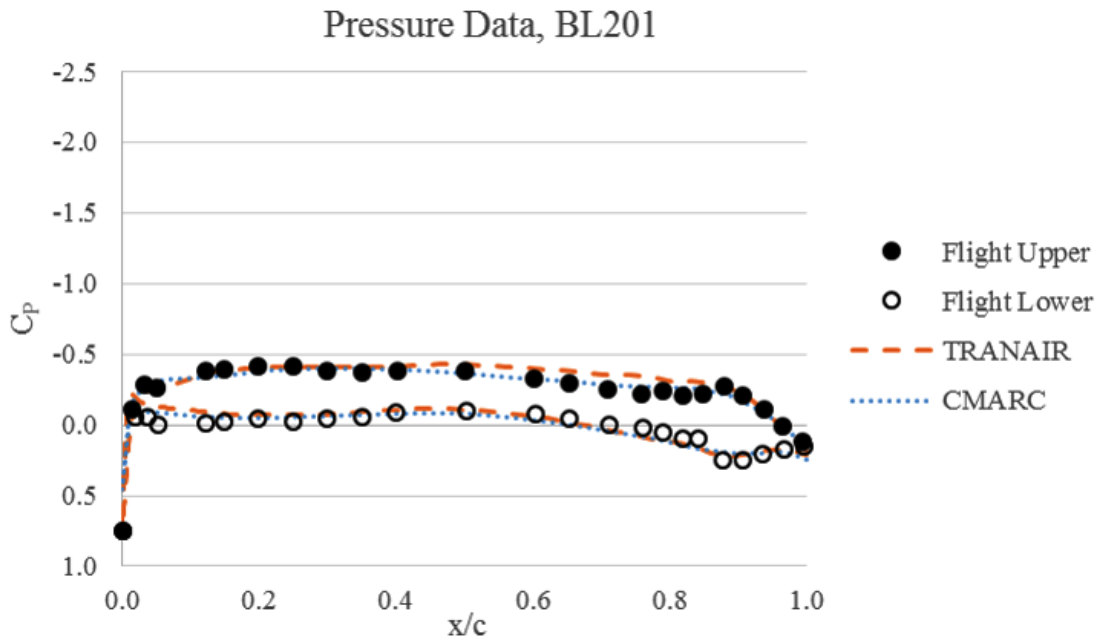
Figure 17. ACTE flap setting at 5 deg, Mach 0.5 at 10,000 ft.

Pressure Data, BL201
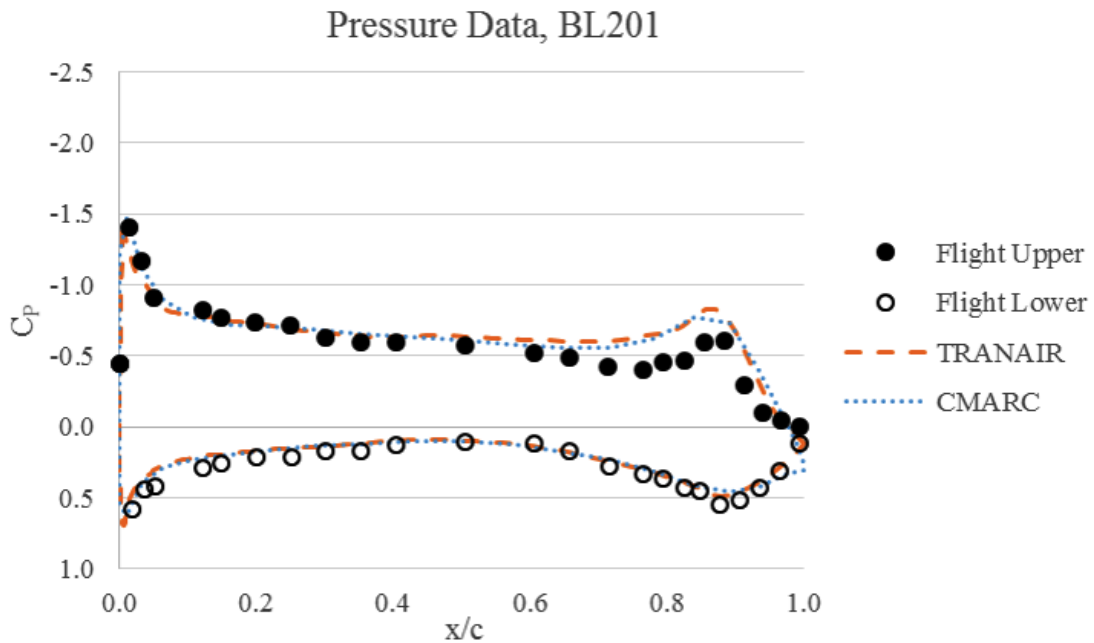
Figure 18. ACTE flap setting at 15 deg, Mach 0.3 at 10,000 ft.

American Institute of Aeronautics and Astronautics

Pressure Data, BL201
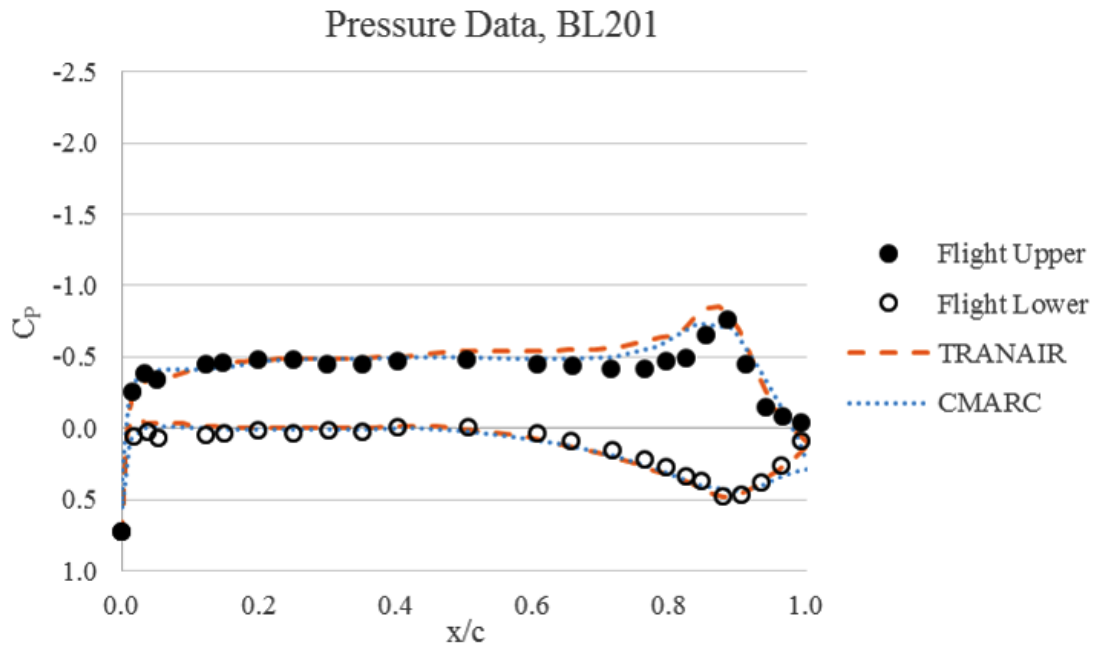
Figure 19. ACTE flap setting at 15 deg, Mach 0.4 at 10,000 ft.

Pressure Data, BL201
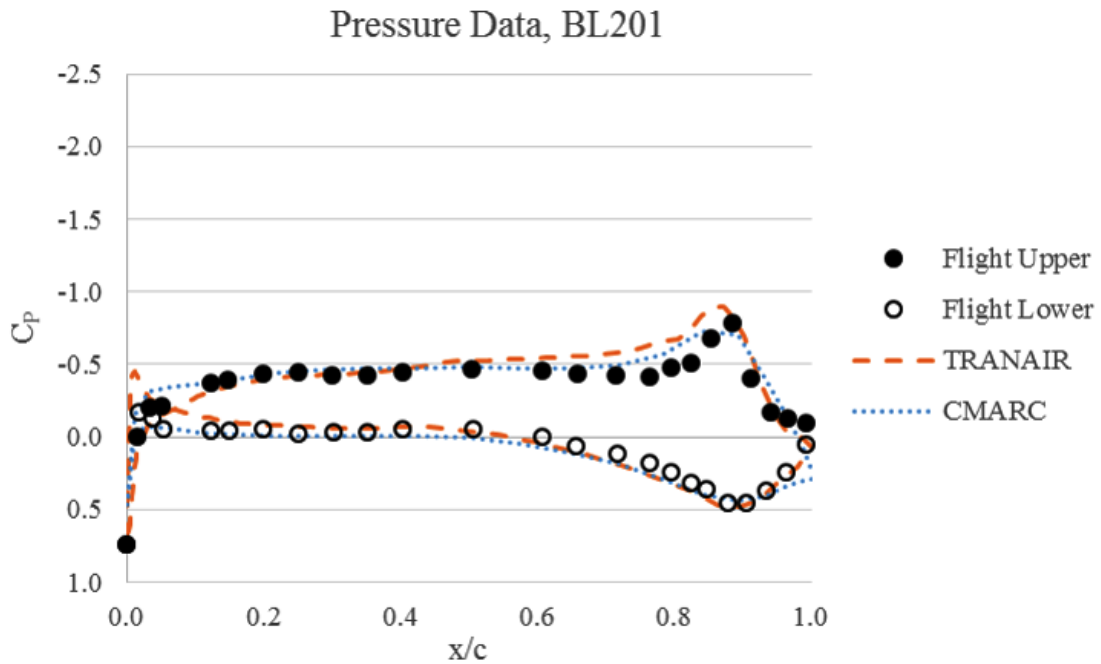
Figure 20. ACTE flap setting at 15 deg, Mach 0.55 at 20,000 ft.

American Institute of Aeronautics and Astronautics
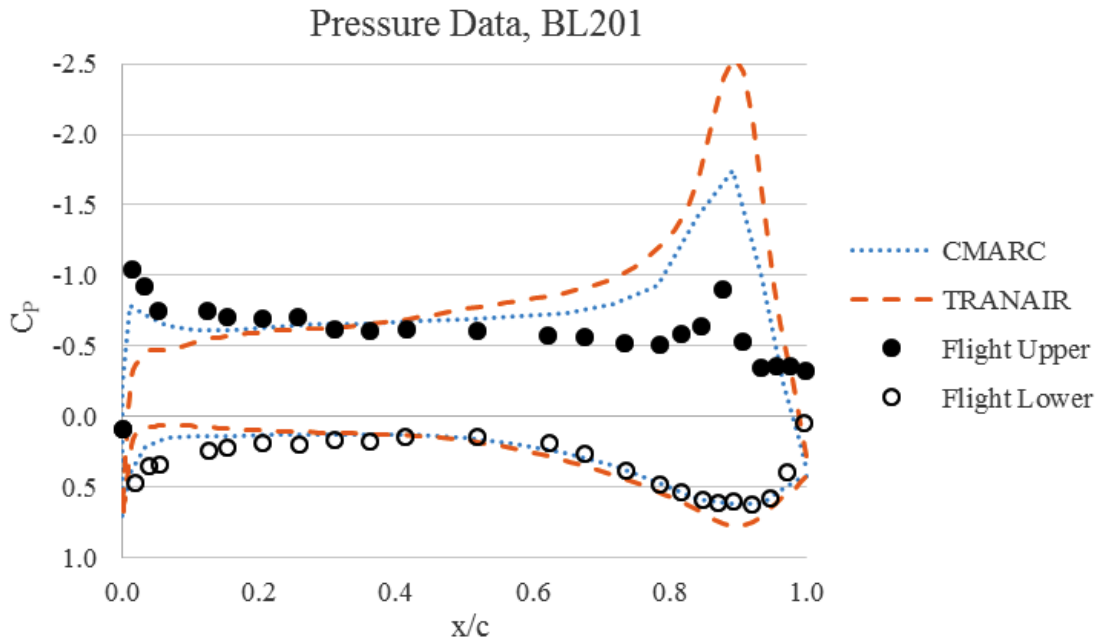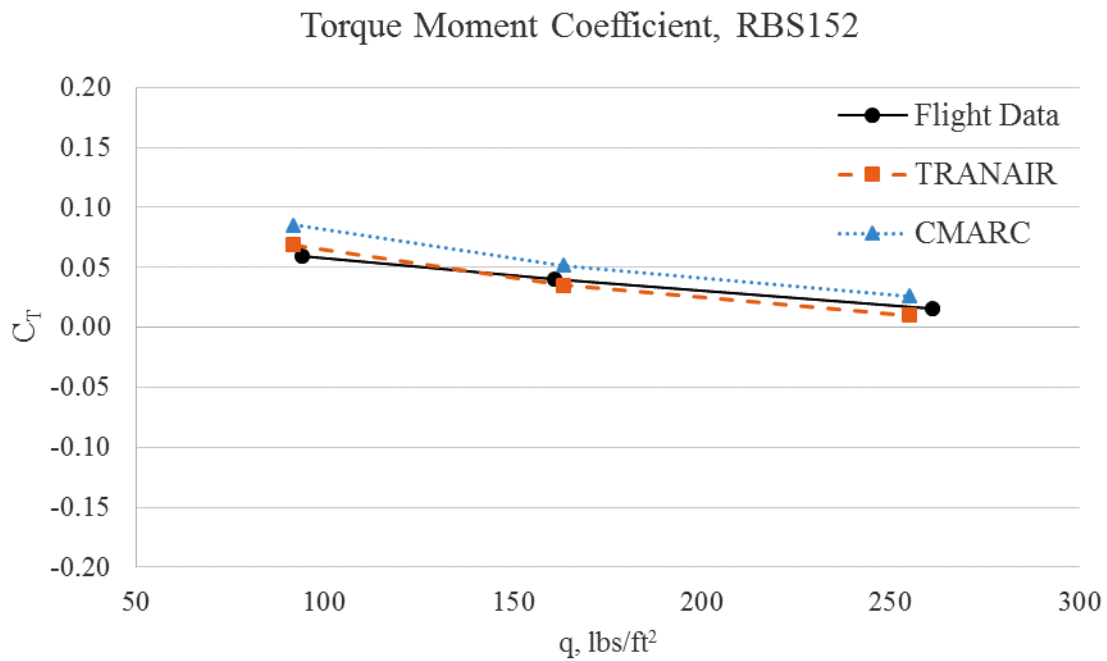
Figure 21. ACTE flap setting at 30 deg, Mach 0.3 at 10,000 ft.
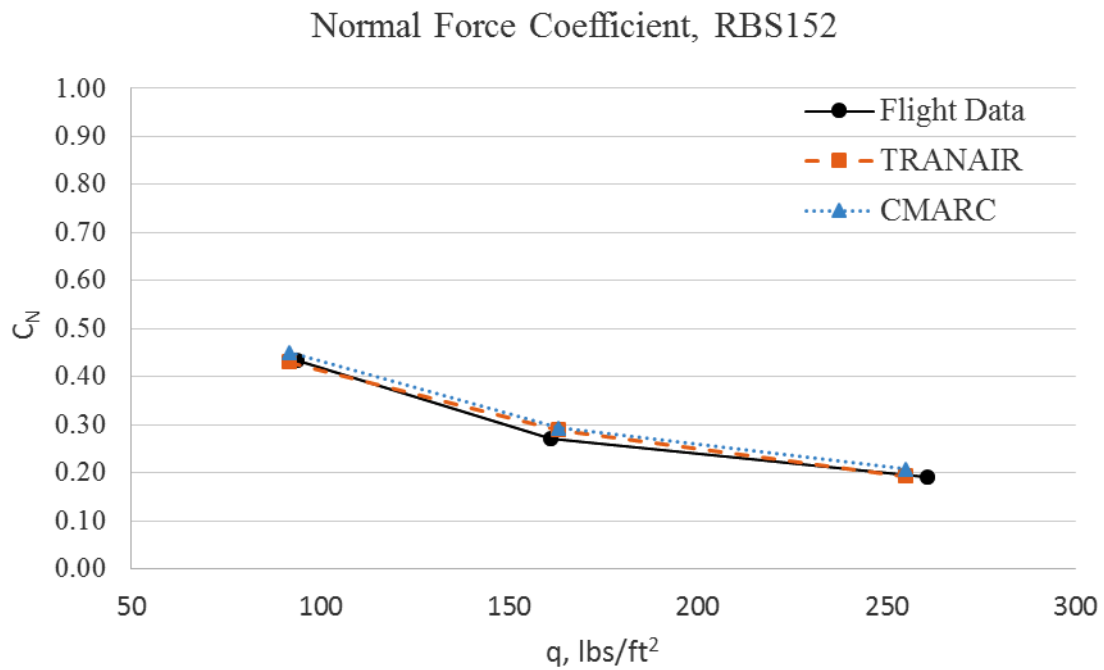
Figure 22. ACTE flap setting at 0 deg.

Normal Force Coefficient, RBS152
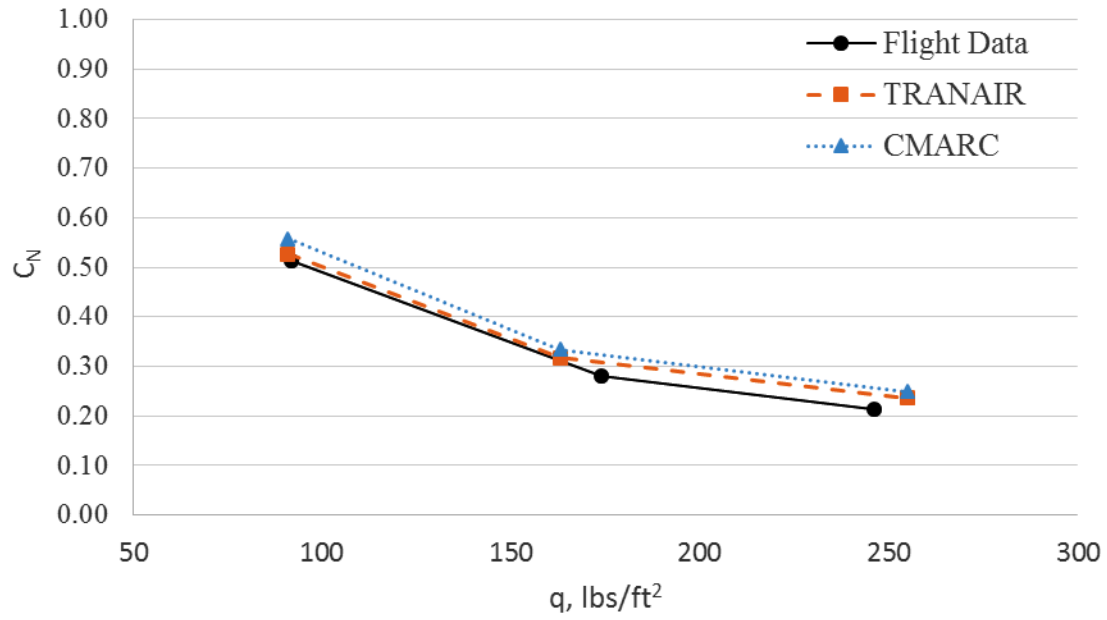
Figure 23. ACTE flap setting at 5 deg.

Normal Force Coefficient, RBS152
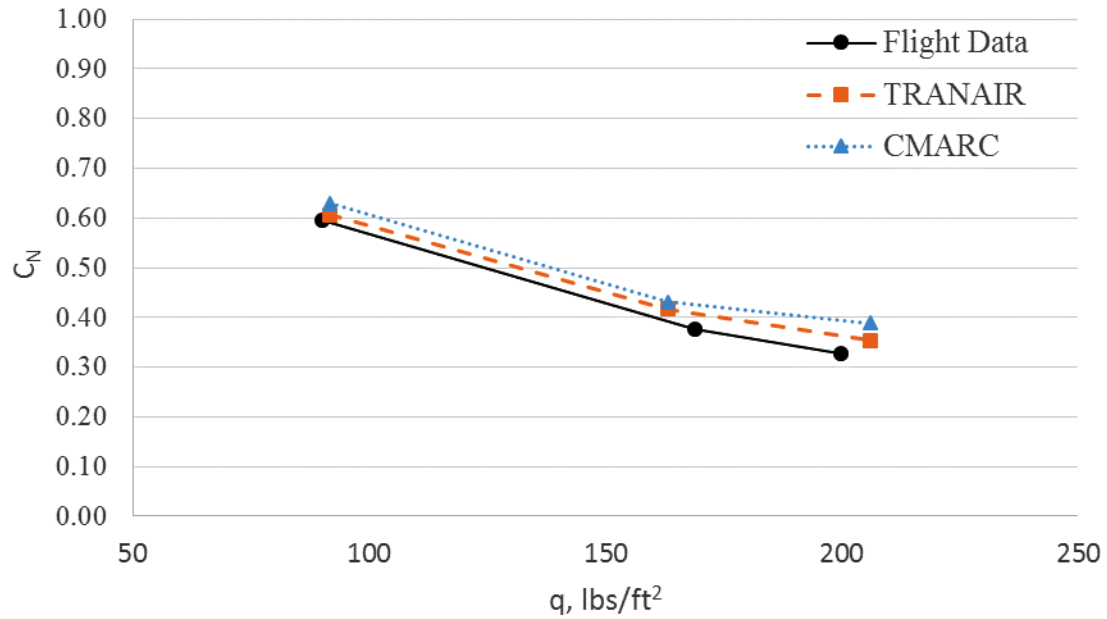
Figure 24. ACTE flap setting at 15 deg.

American Institute of Aeronautics and Astronautics

Bending Moment Coefficient, RBS152
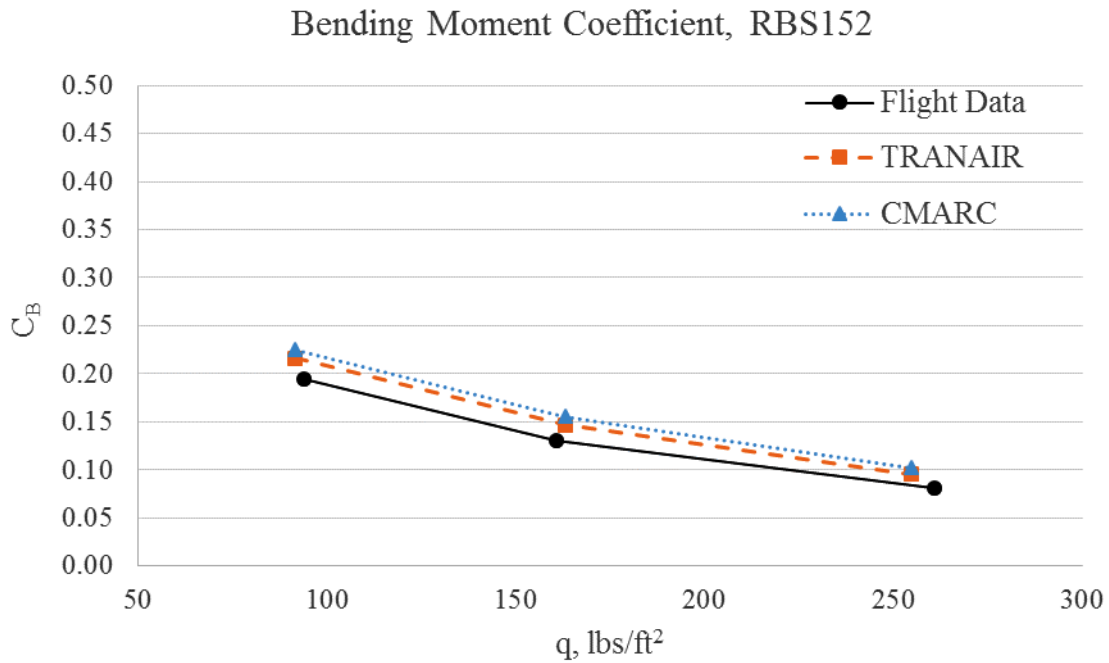
Figure 25. ACTE flap setting at 0 deg.

Bending Moment Coefficient, RBS152
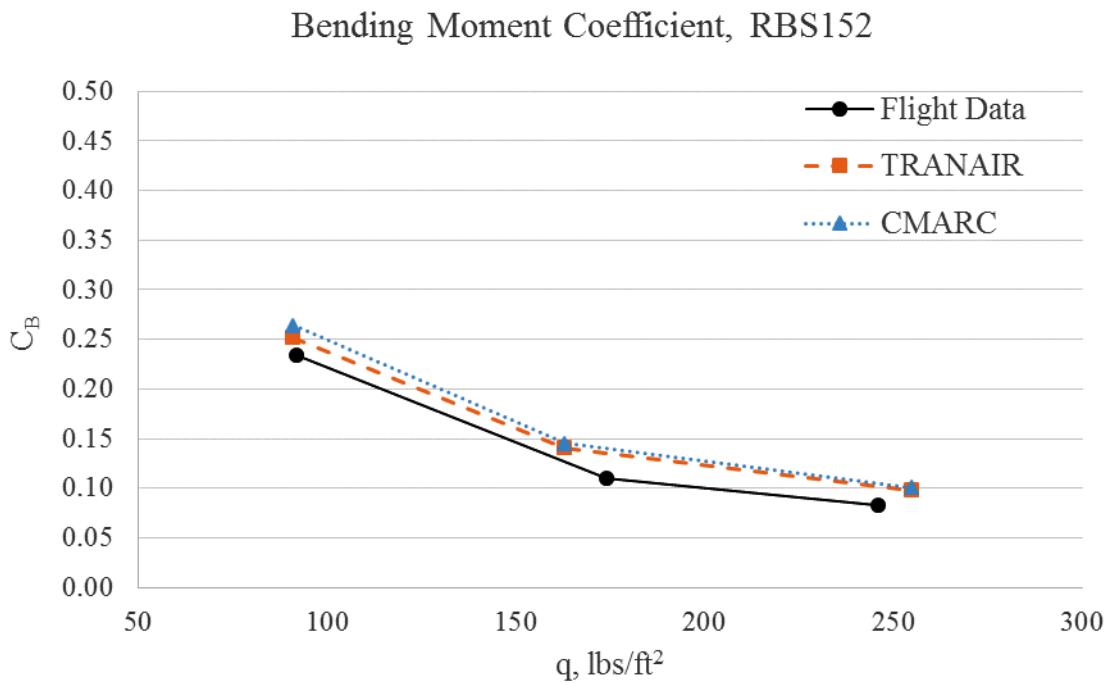
Figure 26. ACTE flap setting at 5 deg.

American Institute of Aeronautics and Astronautics

Bending Moment Coefficient, RBS152

Figure 27. ACTE flap setting at 15 deg.

Torque Moment Coefficient, RBS152

Figure 28. ACTE flap setting at 0 deg.

Torque Moment Coefficient, RBS152
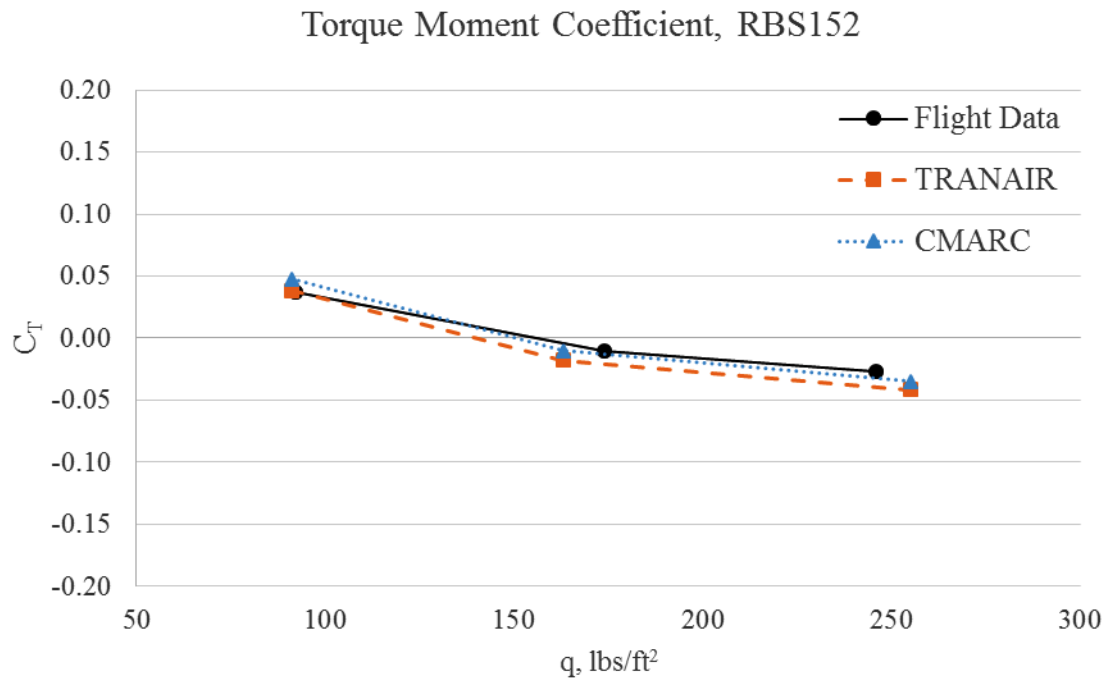
Figure 29. ACTE flap setting at 5 deg.

Torque Moment Coefficient, RBS152
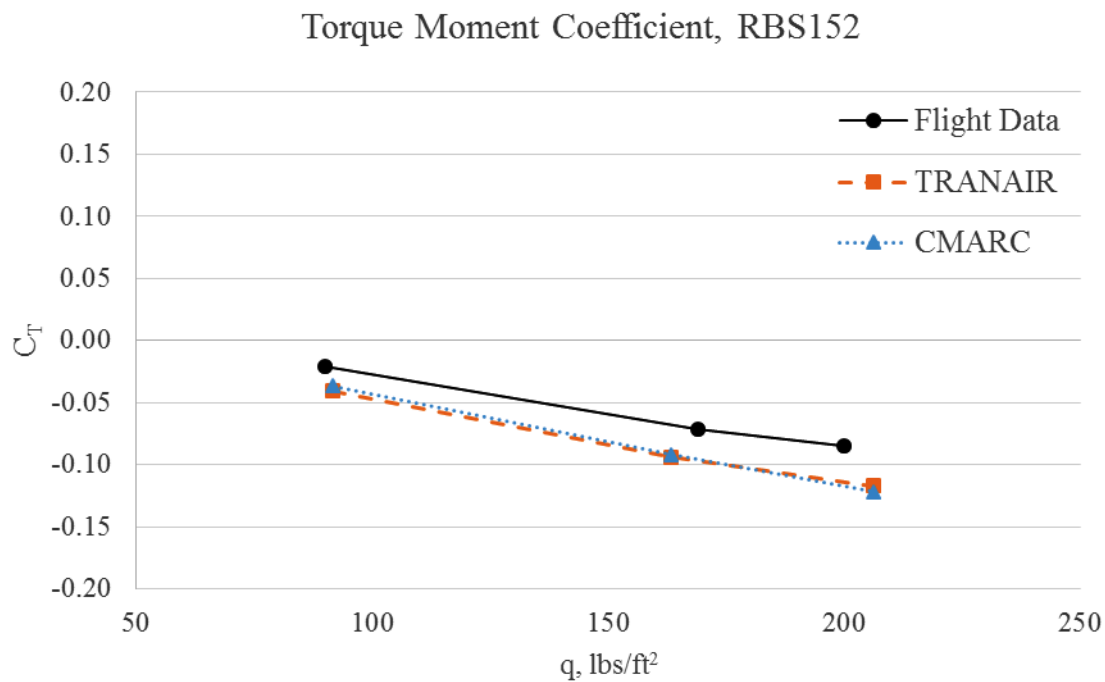
Figure 30. ACTE flap setting at 15 deg.

American Institute of Aeronautics and Astronautics
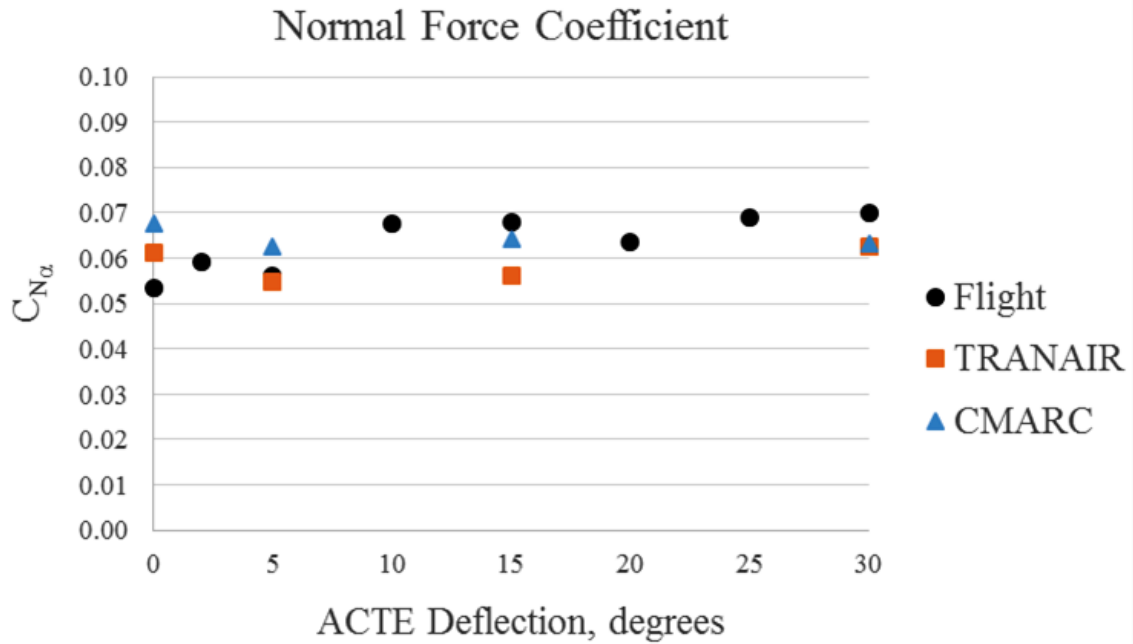
Figure 31. Wing slope normal force coefficient, Mach 0.3, Alt 10,000 ft.
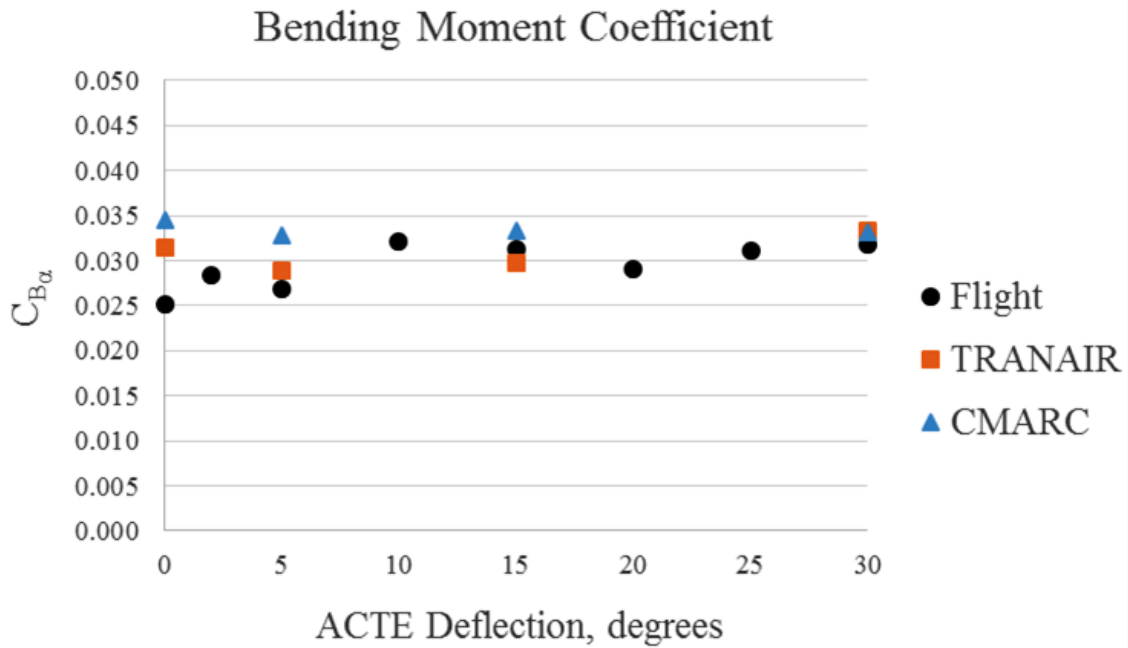
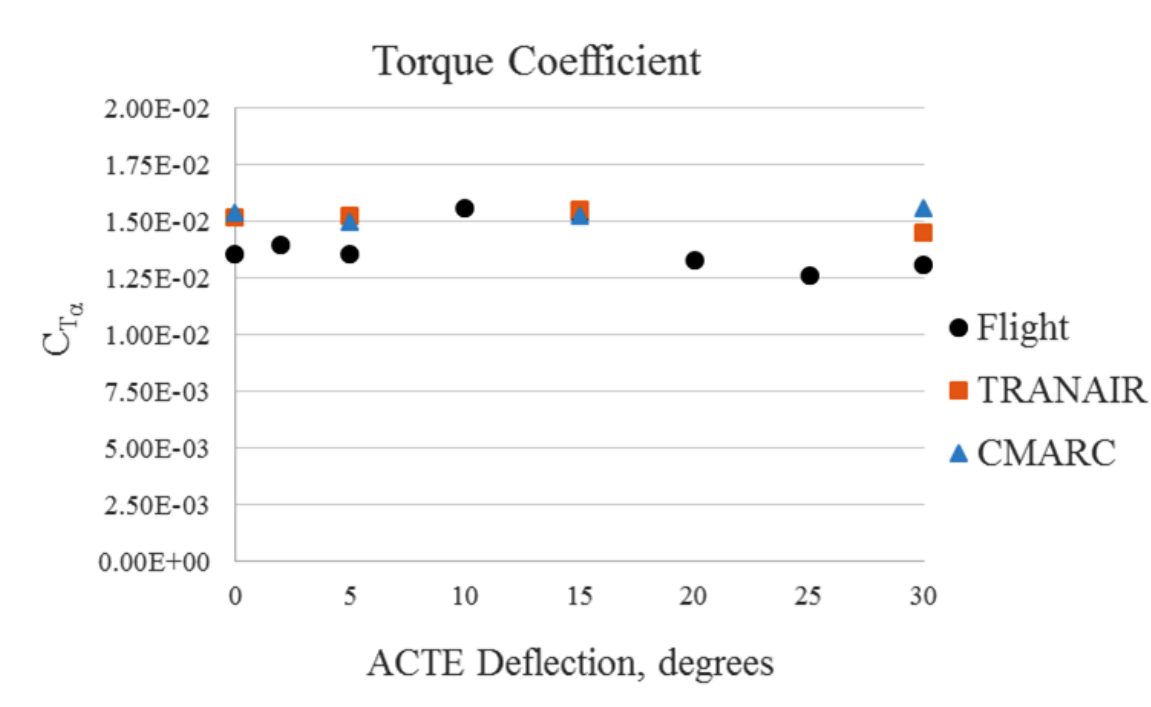**Figure 32. Wing slope bending moment coefficient, Mach 0.3, Alt 10,000 ft.**

American Institute of Aeronautics and Astronautics

Figure 33. Wing slope torque coefficient, Mach 0.3, Alt 10,000 ft.
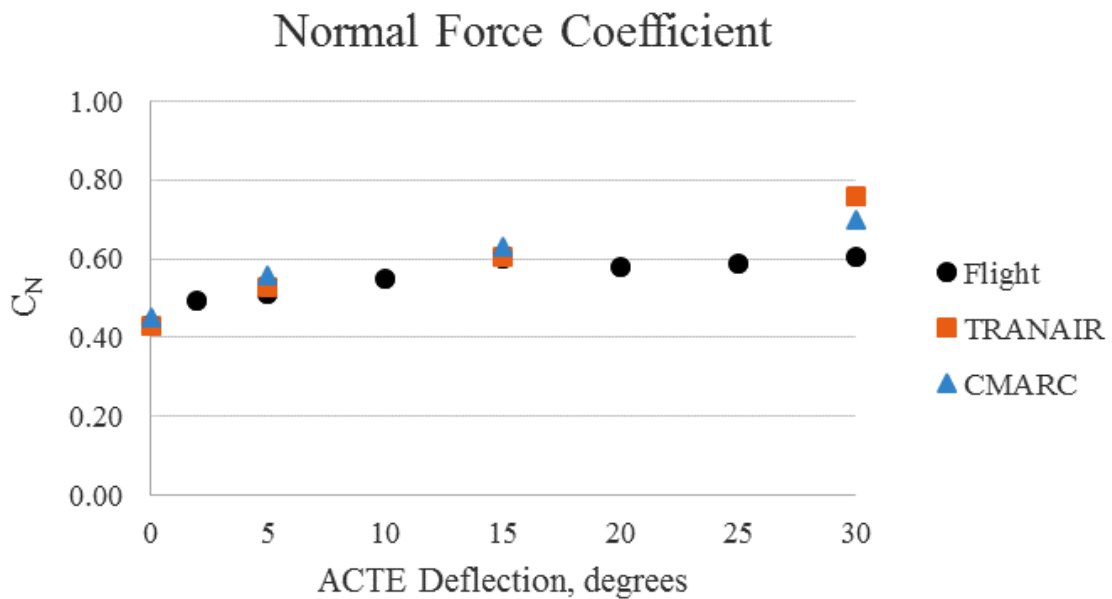
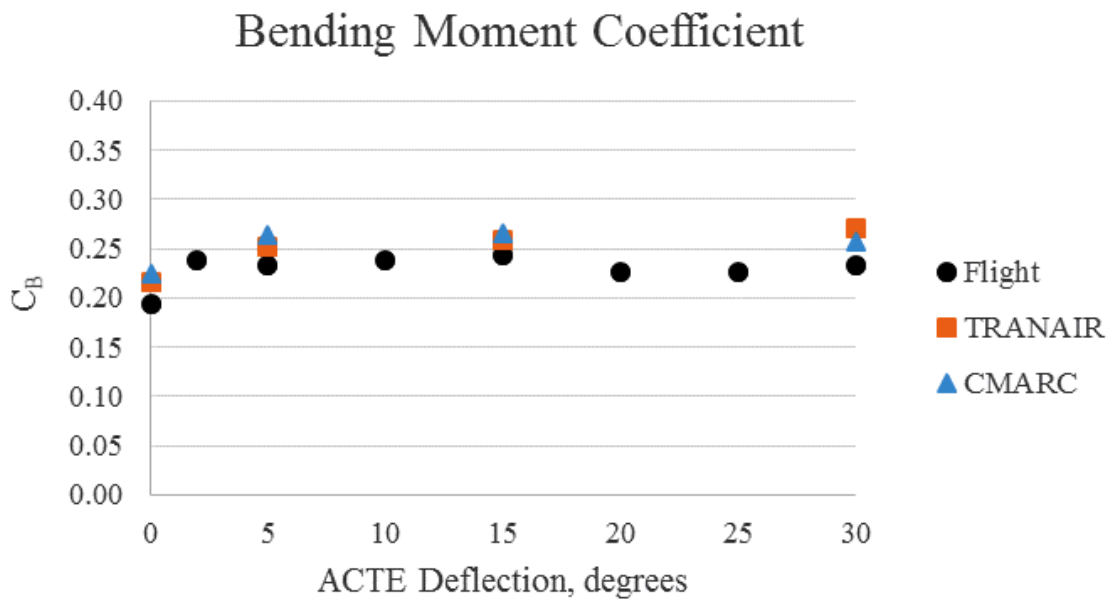**Figure 34. Normal force coefficient, Mach 0.3, Alt 10,000 ft.**

American Institute of Aeronautics and Astronautics

Bending Moment Coefficient

Figure 35. Bending moment coefficient at Mach 0.3, Alt 10,000 ft.
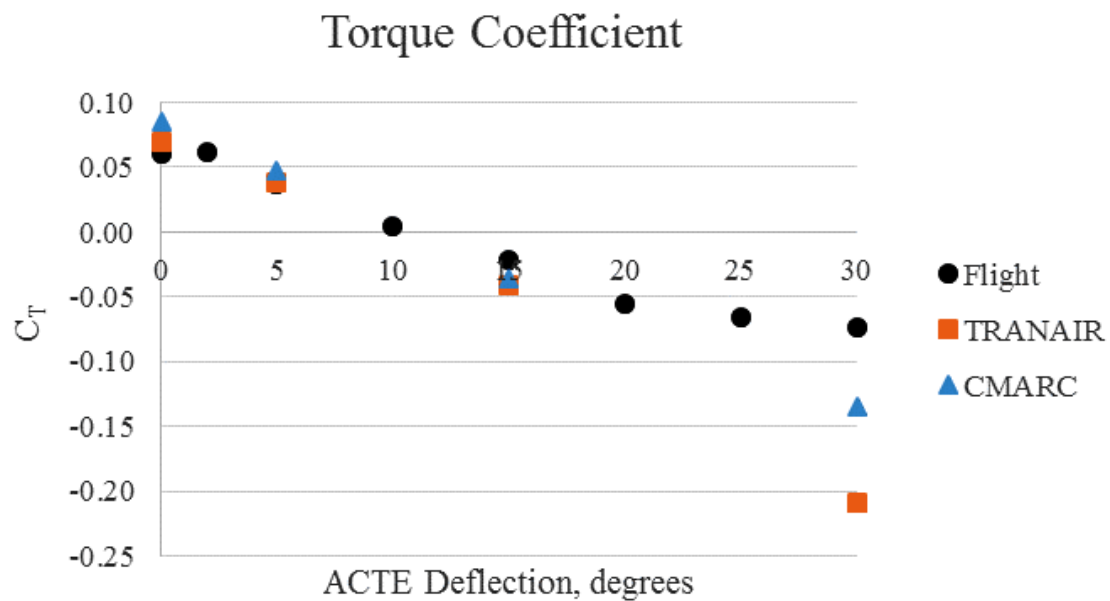
Torque Coefficient

Figure 36. Torque load coefficient at Mach 0.3, Alt 10,000 ft.

American Institute of Aeronautics and Astronautics